View Online / Journal Homepage / Table of Contents for this issue
Dynamic Article Links

Lab on a Chip

Cite this: *Lab Chip*, 2011, **11**, 4221

www.rsc.org/loc

PAPER

Partial-post laplace barriers for virtual confinement, stable displacement, and >5 cm s^{-1} electrowetting transport

E. Kreit,[a] B. M. Mognetti,[bc] J. M. Yeomans[c] and J. Heikenfeld*[a]

Received 11th August 2011, Accepted 7th October 2011
DOI: 10.1039/c1lc20749k

Downloaded by UNIVERSITY OF CINCINNATI on 23 November 2011
Published on 28 October 2011 on http://pubs.rsc.org | doi:10.1039/C1LC20749K

Laplace barriers composed of full-posts or ridges have been previously reported as a mechanism for virtual fluid confinement, but with unstable displacement (capillary fingering or fluid trapping, respectively). A new platform of 'partial-posts' eliminates the disadvantages of full-posts or ridges, while providing ~60–80% open channel area for rapid electrowetting fluid transport (>5 cm s^{-1}). The fluid mechanics of partial-post Laplace barriers are far more complex than previous Laplace barriers as it involves two mechanisms: fluid can first begin to propagate either between, or under, the partial-posts. Careful design of channel and partial-post geometries is required, else one mechanism will dominate over the other. The physics and performance of partial-post Laplace barriers are verified using theoretical equations, experimental results, and dynamic numerical modeling.

Introduction

Laplace barriers[1] are geometrical obstructions which uniquely provide virtual fluid confinement in a channel formed between two parallel plates. Laplace barriers allow confinement of a fluid within any desired geometry, and allow that geometry to be reconfigured on demand through the application of electrowetting[2] or other forces to the fluid (Fig. 1). To date, there is no other mechanism that can utilize voltage to freely manipulate fluid geometry, and maintain that geometry after the voltage is removed. Such capability is significant for applications such as lab-on-chip[3] and displays,[4] and possibly even for reconfigurable antennas.[5] Furthermore, Laplace barriers and electrowetting provide a new experimental platform for the investigation of fluid imbibition.[6] Laplace barriers may also prove useful for virtual confinement in systems without electrowetting, such as conventional, pressure-driven, microfluidic flows.

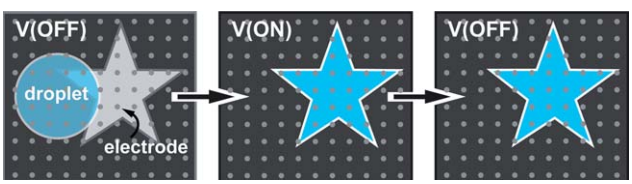


Fig. 1 Representative diagram of Laplace barrier operation with electrowetting actuation. When a voltage is applied the conducting fluid moves to cover the actuated electrodes. When the voltage is turned off it is held in place by the Laplace barriers.

Two distinct types of Laplace barriers (posts and ridges) have been previously reported by our group,[1,3] and explored using electrowetting of aqueous fluids surrounded by oil. Posts extended the entire channel height, while ridges were continuous in the horizontal plane. Posts provided robust geometrical confinement of the fluid, but during fluid transport capillary fingering occurred (and was determined to be theoretically unavoidable).[1] Ridges corrected the capillary fingering issue, but showed slow fluid propagation (~0.2 cm s^{-1}) and oil entrapment between the ridges.

We report here a new design of Laplace barrier (Fig. 2a) which can provide open channel areas exceeding 75%, increase the speed of fluid propagation to >5 cm s^{-1}, decrease oil entrapment, and operate in the stable displacement domain (no capillary fingering). This approach utilizes short posts that do not span the entire channel height, and are therefore referred to as 'partial post' Laplace barriers.

We will show that indicative equations based on simple Laplace theory can be developed to estimate when the interface depins from the posts hence aiding the optimum choice of geometry for the channels. There are two mechanisms in which the fluid can advance: between the posts, or under the posts. Careful design of the channel and partial-post geometries is required, else one mechanism will dominate over the other and the advantages of partial-posts are lost. The analysis we present incorporates experimental results, theoretical equations, and dynamic numerical modeling, all of which confirm the greatly improved capability provided by partial-post Laplace barriers.

[a]*Novel Devices Laboratory, School of Electronics and Computing Systems, University of Cincinnati, Cincinnati, Ohio, 45221, USA. E-mail: heikenjc@ucmail.uc.edu; Fax: +1 5135567326; Tel: +1 5135564763*
[b]*Department of Chemistry, University of Cambridge, Lensfield Road Cambridge, CB2 1EW, United Kingdom. E-mail: bmm411@cam.ac.uk; Fax: +44 (0)1223336262; Tel: +44 (0)1223336471*
[c]*The Rudolf Peierls Centre for Theoretical Physics, 1 Keble Road Oxford, OX1 3NP, United Kingdom. E-mail: j.yeomans1@physics.ox.ac.uk; Fax: +44 (0)1865273947; Tel: +44 (0)1865273992*

Published on 28 October 2011 on http://pubs.rsc.org | doi:10.1039/C1LC20749K
Downloaded by UNIVERSITY OF CINCINNATI on 23 November 2011

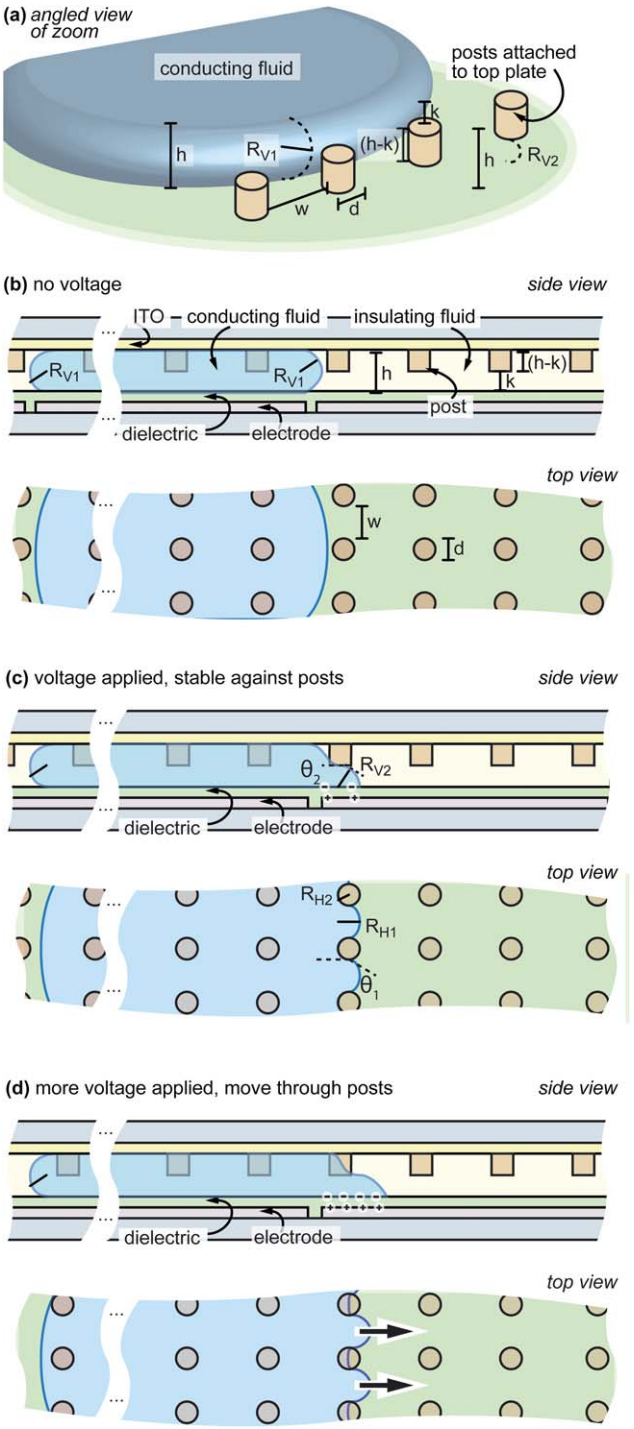


Fig. 2 Schematics of the partial-post Laplace barrier platform (a) angled view of the system; (b) initial position (no voltage applied); (c) voltage applied, the fluid stabilizes against a row of partial-posts; (d) higher voltage applied, the fluid moves past the row of posts.

Materials and fabrication of test devices

Constructing partial-post Laplace barriers with electrowetting control involves very simple fabrication of two glass plates which are then combined with spacers to form an open 50.8x50.8 mm microfluidic channel (Fig. 2b). There is a conventional electrowetting plate for fluid transport, and a Laplace barrier plate for virtual fluid confinement. To create the electrowetting electrode, 100 nm of aluminum was deposited and patterned by photolithography and wet etching. Next, spacers were formed to help set the channel height. These spacers were fabricated by lamination and photolithography of 50 μm thick DuPont™ Per-MX™ 3050. Lamination was performed with a Western Magnum XRL-120 set to 85 °C and 40 PSI lamination pressure. The Per-MX photoresist was photolithographically exposed with 500 mJ cm^{-2} of i-line energy, post exposure baked at 100 °C for 10 min, developed in PGMEA solvent for 5 min, and hard baked at 180 °C for 15 min. The photoresist spacers only need occupy ~1% of the area of a plate. They only set a portion of the channel height as they will press against the partial-post Laplace barriers (together with which they set the total channel height). With the spacer structure in place the electrowetting plate was then conformally coated with 1 μm Parylene C dielectric using a Specialty Coating Systems 2010 lab-coater. To provide hydrophobicity, the electrowetting plate was then dip-coated at 100 mm min^{-1} in a Cytonix Fluoropel 1601V solution and baked for 30 min at 120 °C to form a ~50 nm thick fluoropolymer with 16 mN m^{-1} surface energy.

To create the partial-post Laplace barrier plate, two 50 μm films of the PerMX 3050 were sequentially laminated onto In_2O_3:SnO_2 (ITO electrode) coated glass. This layer was then photolithographically exposed with 900 mJ cm^{-2} i-line exposure energy, and developed and baked. This resulted in a square array of partial-posts of 100 μm height. The Laplace barrier plate was then coated with 50 nm of Fluoropel as previously described. The film of fluoropolymer is so thin that it does not electrically insulate the ITO electrode which was used to provide electrical ground. The conducting fluid used for testing was a custom designed 10 wt% aqueous pigment dispersion prepared by Sun Chemical (~2 cP). The insulating oil used was a blend of Dow Corning OS silicone oils (~ 1.3 cP). The conducting and insulating fluids had a interfacial tension of $\gamma_{ci} \sim 56$mN m^{-1}. For dosing, the conducting fluid was micropipetted near an electrode on the electrowetting plate. Then the partial post plate was lowered on top of the electrowetting plate and the two plates were clamped together. Finally the OS oil was wicked into the channel created between the two plates. Alternately, fluids can be introduced using one of several standard techniques used for lab-on-chip and electrowetting.[7]

Optimization of barrier design

Similar to the previous Laplace barrier designs, the partial-post approach relies on pinning at the posts. The conducting fluid will remain in place unless the interface becomes sufficiently curved that it is able to depin from either the bottom or the sides of the partial-posts. If the interface depins from the sides of the posts it will first move forward between the posts. If however, it first depins from the bottom of the posts, it will first move forward under the posts. We compare this to our previous generations of Laplace barriers. For full posts only the first of these depinning mechanisms is possible, and our previous experiments showed that if the fluid has to diverge around a post a fingering instability results. For Laplace barriers formed of ridges we found that if the conducting fluid only travels under a structure it traps

This journal is © The Royal Society of Chemistry 2011

Published on 28 October 2011 on http://pubs.rsc.org | doi:10.1039/C1LC20749K
Downloaded by UNIVERSITY OF CINCINNATI on 23 November 2011

a significant amount of oil. Moreover it moves slowly since the effective open area of the channel is reduced.

Therefore, to optimise our device we require that the initial depinning takes place under the posts. This is to avoid any fingering instability and to preserve the alignment of the interface. However to avoid fluid trapping we ideally require that the conducting fluid move between the partial-posts before the leading interface reaches the next line of posts. This suggests that the best results will correspond to parameters for which neither depinning route dominates. Having close values for the two pressures is also critical to virtual confinement as if one pressure is considerably smaller it will be the 'weak point' at which the confinement is lost. Another optimization criteria is maximising the open area of the channel to promote rapid fluid transport. We discuss each of these in turn:

Optimization for stable fluid displacement

To help design optimal parameters for the channel we give an estimate of the channel parameters when depinning from the partial posts (fluid advancement) occurs. The Laplace pressure[7] within the conducting fluid is

$$\Delta p = \gamma_{ci}\left(\frac{1}{R_1}+\frac{1}{R_2}\right) \quad (1)$$

This equation takes into account the interfacial surface tension between the conducting and insulating fluids (γ_{ci}) and the principle radii of curvature for the conducting fluid meniscus (R_1, R_2), which depend on the point on the surface at which they are measured and the angles at which the conducting fluid contacts the bounding surfaces.

The structure of the advancing portion of the drop is complex, as shown in Fig. 2. Consider first the portion of the drop between the partial posts. We take a vertical cross section through the conducting fluid, and assume that the meniscus is circular, and makes angles θ_T and θ_B with the top and bottom plates. Recalling that the plates are separated by the channel height h we may estimate the vertical radius of curvature of the drop as

$$R_{v1} = \frac{-h}{(cos\theta_T + \cos\theta_B)} \quad (2)$$

Since the top plate of the system is not an electrowetting plate but is coated with a hydrophobic layer the contact angle on this plate will always be ~180° for the materials we use here. Such a large contact angle is important for the top plate and partial posts, as it reduces pinning for the receding meniscus. The bottom plate is capable of electrowetting[2] modulation and the contact angle on the bottom plate can be calculated as

$$cos\theta_B = \frac{\gamma_{id}-\gamma_{cd}}{\gamma_{ci}} + \frac{C\cdot V^2}{2\gamma_{ci}} \quad (3)$$

where C is the capacitance per unit area of the hydrophobic dielectric (d) and V is the applied DC or AC rms voltage. The typical range of contact angle modulation of conducting aqueous fluids (c) in insulating oil (i) is from 180° to ~60°, beyond which contact angle saturation dominates.[8] We assume a typical value of 90° below.

Next, we consider the top view of the channel so we can estimate the horizontal radius of curvature. This is determined by the post distance (w) and the angle (θ_1) between the interface at the point at which it collides with the post and the flow direction (Fig. 2c). θ_1 determines the fraction of the post which is wetted by the conducting fluid. Then the horizontal radius of curvature of the part of the interface between the posts can be estimated in a similar way as

$$R_{h1} = \frac{-w}{(2cos\theta_1)} \quad (4)$$

Using eqn (2) and (4) in eqn (1) with $\theta_T = 180$ and $\theta_B = 90$ we obtain the following Laplace pressure:

$$\Delta p_b = \gamma_{ci}\left(\frac{1}{h}-\frac{2cos\theta_1}{w}\right) \quad (5)$$

For the limiting case corresponding to the maximum possible interface curvature ($\theta_1 = 180°$), an estimate for *the threshold pressure for depinning between the posts* is

$$Between\ posts: \Delta p_b^{tr} = \gamma_{ci}\left(\frac{1}{h}+\frac{2}{w}\right) \quad (6)$$

Next, and similarly, to obtain an estimate for depinning from the bottom of (under) the posts, we consider the interface shape below a post. Now

$$R_{v2} = \frac{-k}{(cos\theta_2 + cos\theta_B)} \quad (7)$$

where θ_2 is the angle the interface makes with the bottom of the posts (Fig. 2c). For $\theta_2 < 180°$ the interface remains pinned to the back edge of the post. Verified by the numerical modeling (see later section) which shows that the interface is concave, we estimate the horizontal curvature as

$$R_{h2} = \frac{-d}{2} \quad (8)$$

Therefore, again choosing $\theta_B = 90$ we obtain:

$$\Delta p_u = \gamma_{ci}\left(\frac{-2}{d}-\frac{\cos\theta_2}{k}\right) \quad (9)$$

For the limiting case corresponding to the maximum possible interface curvature ($\theta_2 = 180°$), an estimate for *the threshold pressure for depinning under the posts* is

$$Under\ posts: \Delta p_u^{tr} = \gamma_{ci}\left(\frac{-2}{d}+\frac{1}{k}\right) \quad (10)$$

To this point we have only discussed the thresholding pressures to prevent capillary fingering for the advancing meniscus. For completeness it is worth mentioning that the pressure required for droplet transport past the partial posts, must take into account the driving pressure provided by the receding meniscus. Since the receding meniscus is not electrowetted this pressure is determined by the channel height and is given by:

$$\Delta p_R = \gamma_{ci}\left(\frac{2}{h}\right) \quad (11)$$

When $\Delta p_R > \Delta p_b^{tr}$ or Δp_u^{tr} then the fluid will be able to move past the partial posts. Otherwise it will remain confined by the partial posts.

To graphically determine ideal geometries, MATLAB was used to create multivariable plots showing the difference

Published on 28 October 2011 on http://pubs.rsc.org | doi:10.1039/C1LC20749K
Downloaded by UNIVERSITY OF CINCINNATI on 23 November 2011

between the threshold pressures $\Delta p_b^{tr} - \Delta p_u^{tr}$. For sake of simplicity, and for practical reasons, several variables were fixed. The channel height was set to h = 150 μm. This height is similar to that used in traditional electrowetting lab-on-chip[6] applications with ~1 × 1 mm^2 electrode areas. This aspect ratio for electrode and channel height supports rapid transport speeds,[9] and the height is small enough to allow strong virtual confinement of the conducting fluid. The next assumption was that the posts height (h-k) and width (d) were equal for easy (repeatable) fabrication using photolithography or micro-replication. Lastly, the electrowetting was set to $\theta_B = 90°$, an angle that is easily achieved before electrowetting saturation[8] and/or hydrophobic dielectric damage. Utilizing these assumptions, Fig. 3a provides a plot of the difference between the threshold pressure for advancing between Δp_b^{tr} and the threshold pressure for moving under Δp_u^{tr} the partial-posts, using eqn (6) and (10). $\Delta p_b^{tr} - \Delta p_u^{tr}$ is plotted as a function of both the width of the post (d), and the spacing between posts (w). A positive value of $\Delta p_b^{tr} - \Delta p_u^{tr}$ is desired, such that the conducting fluid will move forward under the partial-posts before it depins from the sides of the partial posts. This constraint for $\Delta p_b^{tr} - \Delta p_u^{tr}$ gives a wide range of possible geometries, but does not take into account open channel area or virtual confinement which we discuss now.

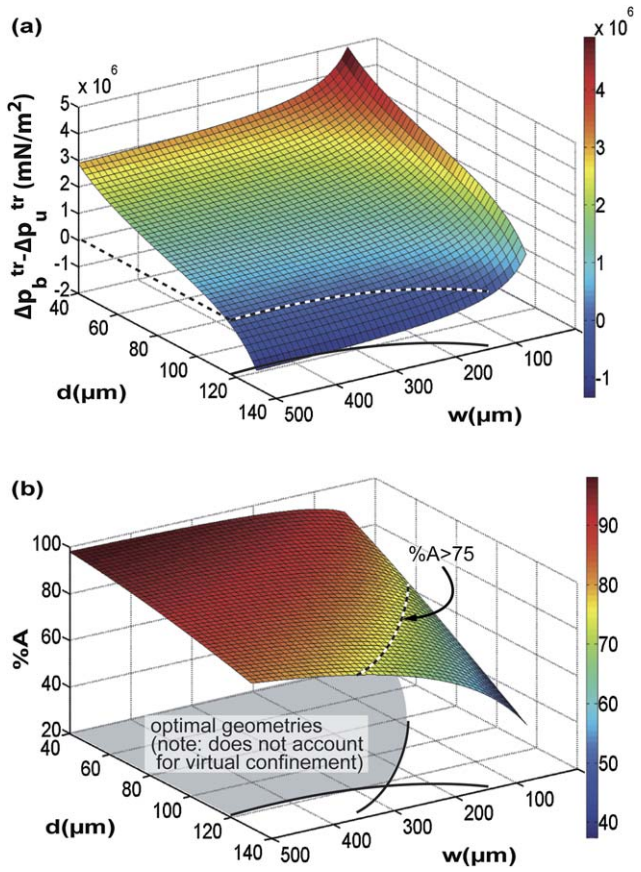


Fig. 3 (a) difference between the threshold pressures for depinning between and under the posts $\Delta p_b^{tr} - \Delta p_u^{tr}$ (b) percent of open area of a unit cell of the array of partial-post Laplace barriers. The plots also include dotted and solid lines to indicate the limits of the desirable geometries.

Optimization for rapid fluid transport

In order to calculate the percentage of open channel (which will effect fluid transport speed), the cross sectional area was calculated as (1 − (partial-post area)/(the total channel area)). In the derivation, (h-d) is substituted for k, and the equation is then simplified to obtain:

$$\%A = \frac{hw + dh - d^2}{h(w+d)} \times 100 \qquad (12)$$

Fig. 3b shows this equation plotted against the same geometric variables d and w. For fastest fluid transport, it is desirable to have the highest possible percentage of open channel area. As can be seen from purely geometric considerations, %A>75% is possible. In the bottom plane of Fig. 3b, the limits of desirable geometries are combined from Fig. 3a and 3b.

Ensuring virtual confinement

The last goal of geometrical optimization is to provide strong virtual confinement so that the fluid can be held in any geometrical configuration without an applied voltage. For a given channel height and post width, confinement against depinning between or under the posts is optimized by minimizing the distance between the posts w or the length of the gap under the posts k respectively. The radius of curvature of the liquid that bows out between the posts is estimated in eqn (4). Assuming that for stability $\cos\theta_1$ is bounded by 180°, gives $R_{h1} \geq w/2$ This means that the best confinement obtainable for the system is controlled by the selected post pitch w. Virtual confinement will be most difficult when the interface lies at an angle to the principle axes of the post lattice, hence the star shape in Fig. 1 is a demanding example.

Experimental results

Utilizing the optimization parameters, and factoring in fabrication constraints, the following geometry was selected for testing: w = 100 μm, d = 100 μm, h = 150 μm, k = 50 μm. These parameters provide a $\Delta p_b^{tr} - \Delta p_u^{tr}$ of ~1.5 kN m^{-2}, and a %A of 67%. These are excellent parameters providing all three desired outcomes: stable fluid displacement, potential for rapid transport, and strong virtual confinement. Fig. 4 shows experiments with full-posts and partial-posts, confirming stable displacement for the case of partial posts. High speed video was also taken at 5000 fps in order to calculate the transport speed. An average of 10 measurements gave a result 4.3 ± .2 cm s^{-1}, with maximum transport speeds exceeding 5 cm s^{-1}, for an applied electromechanical energy of 85 mJ m^{-2}. This level of electromechanical energy requires 80 V with a 1 μm Parylene C dielectric and 25 V if a 100 nm Si_3N_4 dielectric is used.

To test the virtual confinement for the partial post platform the same set of parameters were utilized in conjunction with a star-shaped electrode. The results of this test are seen in Fig. 5. The electrode was cycled ON/OFF five times before the voltage OFF photographs were taken. The higher magnification images reveal the virtual confinement and slight (but evenly distributed) protrusion of the conducting fluid between the partial-posts. The results also show that the partial-post array does not need to be

 This journal is © The Royal Society of Chemistry 2011

Published on 28 October 2011 on http://pubs.rsc.org | doi:10.1039/C1LC20749K
Downloaded by UNIVERSITY OF CINCINNATI on 23 November 2011

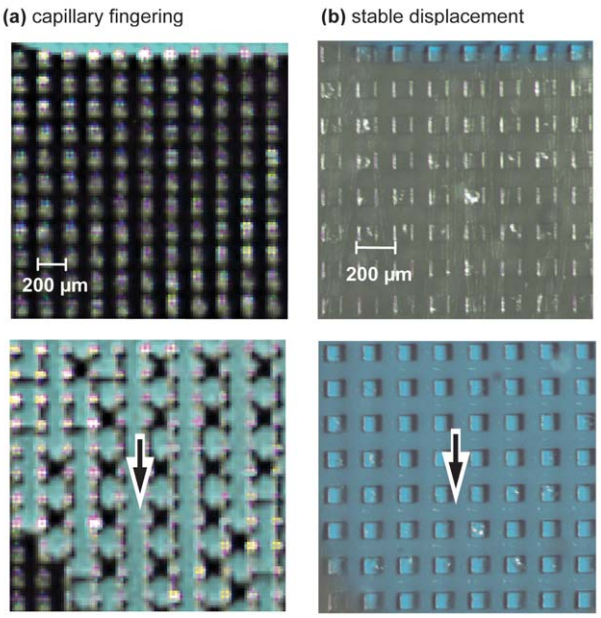


Fig. 4 Regimes of electrowetting transport through Laplace barriers with: (a) full-posts showing capillary fingering (k = 0) from; (b) partial-posts showing stable displacement. The blue fluid is the conducting fluid.

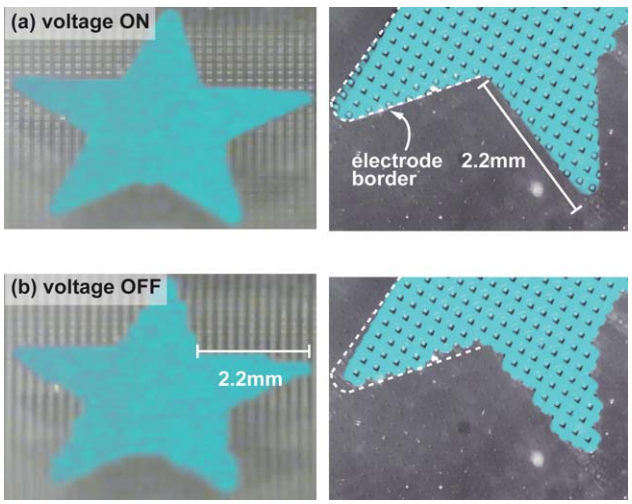


Fig. 5 Operation of partial post Laplace barrier platform (a) voltage on (~50 mJ m^{-2}); (b) voltage off. The images at right are zoom-in photographs of the same image at left. The blue fluid is the conducting fluid.

aligned in any particular fashion with the electrowetting electrode, although a small degree of stepping is observed if the meniscus is not aligned with a lattice axis. Because no-alignment is needed, any group pursuing electrowetting lab- on-chip[7] devices can easily integrate a top-plate with partial posts and achieve the results detailed here.

A transport test was also performed by moving an entire droplet between two electrode paths of 1 × 2 mm dimension. The results are seen in Fig. 6, and the reader is reminded that transparent ITO electrodes were utilized. The lighter color is simply the optical shadow cast by the darker (blue) conducting fluid.

The results show excellent virtual confinement in rectangular geometries that match the electrode size. As visible in Fig. 6b, during transport the receding meniscus exhibits some elongation, but this is also observed for conventional electrowetting transport without Laplace barriers. The elongated portion will always rejoin the bulk of the fluid (Fig. 6c).

Secondary effects and numerical modeling results

There are several observable secondary effects that could not be explained by the simple Laplace theory described in the previous sections. Therefore dynamic numerical modeling was also explored. At micron length scales models with atomistic resolution are not feasible and mesoscopic descriptions are appropriate. Thus a binary fluid model was quantified by two local fields: the fluid density $n = n_c + n_i$ and the concentration $\phi = n_c + n_i$ where n_c and n_i are the densities of the conducting and insulating fluids respectively. The equilibrium properties of the fluids were described by the free energy functional:

$$\psi = \int_{\Omega} \left(\frac{c}{3} n \log n + \frac{k}{2} (\delta_{\alpha} \phi)^2 - \frac{A}{2} \phi^2 + \frac{A}{4} \phi^4 \right) + \int_{\delta\Omega} h \cdot \phi \qquad (13)$$

The first integral of eqn (13) accounts for the thermodynamics of the fluid in the bulk. In particular k and A regulate the surface tension and the interface thickness. The integral along the boundary of the micro channel ($\delta\Omega$) controls the wettability properties of the system through an external field h that is uniquely determined by the Young's contact angle (θ_Y).[10] The equilibrium configuration of the fluid corresponds to the minimization of the free energy in the system.

The time evolution of the fluid velocity ν and density n obey the Navier–Stokes equations, while the order parameter ϕ follows a convection-diffusion equation. These equations of motion are solved using well established lattice Boltzmann algorithms.[11–13] Full details of these equations and the numerical scheme have been previously published.[14,15]

The results of the modeling (Fig. 7) show that the fluid is moving as previously predicted. The fluid first moves under a post (Fig. 7a) and then, as the fluid meniscus continues to advance to the next set of partial-posts, the fluid moves between the posts (Fig. 7b). Although the model did show these predicted modes of fluid flow, it also produced an unexpected result. It is clear in Fig. 7b that as the conducting fluid continued to advance past the partial-posts, the conducting fluid pulls further and further away from the top plate.

An experiment was designed to specifically validate this unexpected result (conducting fluid pulling away from the top plate). In this experiment the insulating fluid (oil) was dyed opaque black to allow improved visual identification of fluid positions and oil trapping (Fig. 8). As the fluid was moving from one pad to another, the advancing meniscus of the fluid could be seen propagating under the posts faster than between them (Fig. 8b). The photograph in Fig. 8b is a top view through the transparent partial-posts. The red outlined area clearly shows the blue conducting fluid in contact with the bottom of the partial-posts, but not in contact with the top-plate. This confirms the flow pattern predicted by the numerical modeling. It is undesirable as it will reduce the maximum achievable transport flux as only a portion of the available channel area is being used for

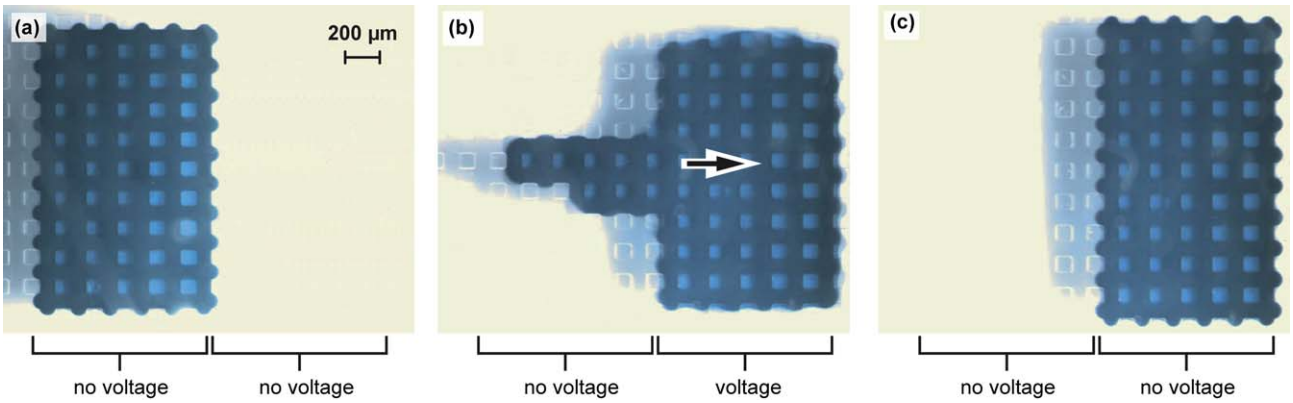


Fig. 6 Time lapse image showing the movement of a droplet between two electrodes in a field of partial-posts (a) both electrodes off; (b) voltage on right electrode (~50 mJ m^{-2}) with voltage on left electrode off; (c) both electrodes off. Blue fluid is the conducting fluid.

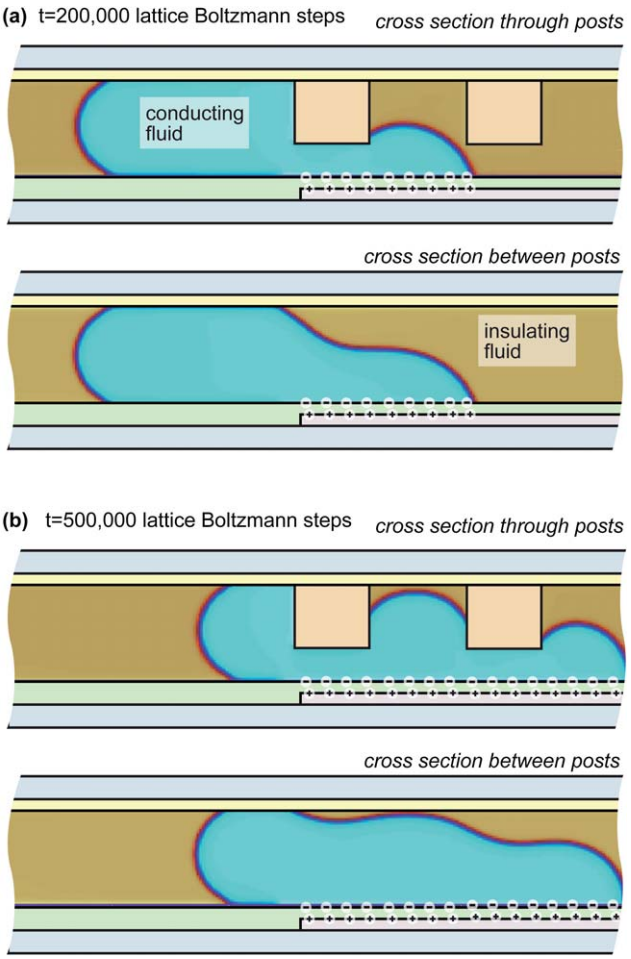


Fig. 7 Modeling results showing the motion of a fluid droplet past a partial-post Laplace barrier. Vertical cross sections at the center of the posts and mid-way between the posts are plotted for.

transport. This is also why in Fig. 6b the total apparent area of the conducting fluid during transport (and perceived volume), exceeds the total area at rest (and perceived volume) in Fig. 6a,c. Preliminary work has shown that these undesirable secondary effects can be eliminated by only slightly reducing the post width

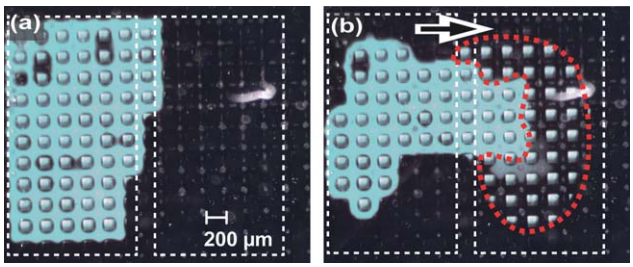


Fig. 8 Blue conducting fluid tests in a black oil ambient with a value for *w* that is non-ideal (too small). The white outlines depict electrode pad boundaries. The red outline depicts the area of non-ideal flow. In (a) the voltage is off for both electrode pads, and in (b) voltage is provided only to the electrode path at the right and a snapshot is captured of the fluid as it moves between electrodes.

(d) or increasing the spacing between the posts (w) by ~10–20% of the values reported herein.

Conclusions

We have demonstrated a new design of partial-post Laplace barriers which eliminate capillary fingering and significantly decrease oil entrapment, improve transport speed, and provide strong virtual confinement. A static theoretical model based purely on contact angles and Laplace pressure was shown to be experimentally valid, but insufficient for predicting undesirable secondary effects found with numerical modeling. Partial-post Laplace barriers appear to be an attractive solution for virtual confinement, and are very easily integrated onto conventional electrowetting transport plates. Along with new scientific understanding, this work may provide practical advances in reconfigurable lab-on-chip,[3] electronic displays,[4] and agile antennas.[5] These results may also prove useful for those exploring mechanisms for virtual confinement in systems without electrowetting such as conventional pressure-driven microfluidic flows.

Acknowledgements

The Univ. Cincinnati authors gratefully acknowledge partial support from NSF Career award no. 0640964 (University of Cincinnati), NSF IHCS award no. 1001141, AFRL contract no. 5408-25-SC-0003 (Rajesh Naik), and an ARL grant no.

Downloaded by UNIVERSITY OF CINCINNATI on 23 November 2011
Published on 28 October 2011 on http://pubs.rsc.org | doi:10.1039/C1LC20749K

This journal is © The Royal Society of Chemistry 2011

W9111NF-09-2-0034 (Dave Morton and Eric Forsythe). The Oxford authors acknowledge support from the US Office of Naval Research.

Notes and references

1 E. Kreit, M. Dhindsa, S. Yang, M. Hagedon, K. Zhou, I. Papautsky and J. Heikenfeld, *Langmuir*, 2010, **26**(23), 18550–18556.
2 F. Mugele, A. Klingner, J. Buehrle, D. Steinhauser and S. Herminghaus, *J. Phys.: Condens. Matter*, 2005, **17**, S559–S576.
3 M. Dhindsa, J. Heikenfeld, S. Kwon, J. Park, P. D. Rack and I. Papautsky, *Lab Chip*, 2010, **10**, 832–836.
4 S. Yang, J. Heikenfeld, E. Kreit, M. Hagedon, K. Dean, K. Zhou, S. Smith and J. Rudolph, *JSID*, 2011, **19**(9), 608–613.
5 R. K. Mohammed, G. J. Hayes, J. So, G. Lazzi and M. D. Dickey, *Applied Physics Letters*, 2011, **99**, 0135011–3.
6 M. L. Blow, H. Kusumaatmaja and J. M. Yeomans, *J. Phys.: Condens. Matter*, 2009, **21**, 464125.
7 J. Berthier, *Microdrops and Digital Microfluidics*, William Andrew Publishing, NY, 2008.
8 S. Chevalliot, S. Kuiper, and J. Heikenfeld, *Experimental Validation of the Invariance of Electrowetting Contact Angle Saturation*, JAST Special Issue on Electrowetting, DOI: 10.1163/156856111x599580.
9 J. H. Song, R. Evans, Y. Y. Lin, B. N. Hsu and R. B. Fair, *Microfluid. Nanofluid.*, 2009, **7**, 75–89.
10 J. W. Cahn, *J. Chem. Phys.*, 1977, **66**, 3667.
11 S. Succi, *The Lattice Boltzmann Equation, for Fluid Dynamics and Beyond*, Oxford University Press: Oxford, 2001.
12 J. M. Yeomans, *Phys. A*, 2006, **369**, 159.
13 M. R. Swift, E. Orlandini, W. R. Osborn and J. M. Yeomans, *Phys. Rev. E: Stat. Phys., Plasmas, Fluids, Relat. Interdiscip. Top.*, 1996, **54**, 5041.
14 H. Kusumaatmaja and J. M. Yeomans, *Simulating Complex Systems by Cellular Automata*, 2010, A. G. Hoekstra, *et al.* (editors), Springer, 2010.
15 B. M. Mognetti and J. M. Yeomans, *Phys. Rev. E: Stat., Nonlinear, Soft Matter Phys.*, 2009, **80**, 056309.

Published on 28 October 2011 on http://pubs.rsc.org | doi:10.1039/C1LC20749K
Downloaded by UNIVERSITY OF CINCINNATI on 23 November 2011